Partially dealuminated heulandite produced by acidic REECl₃ solution: A chemical and single-crystal X-ray study

Tobias Wüst, Jano Stolz, and Thomas Armbruster*

Laboratorium für chemische und mineralogische Kristallographie, Universität Bern, Freiestrasse 3, CH-3012 Bern, Switzerland

ABSTRACT

Single crystals (0.1–0.5 mm) of natural heulandite from Nasik (India) were treated in 4 M NaCl solution at 423 K for 12 weeks, yielding almost fully Na-exchanged heulandite (composition: $Na_{8.44}Ca_{0.09}K_{0.01}[Al_{8.63}Si_{27.37}O_{72}]\cdot nH_2O$). This precursor phase was subsequently treated in a Teflon autoclave with 0.5 M rare-earth element (REE) solution (0.25 M $ErCl_3\cdot6H_2O$ and 0.25 M $LaCl_3\cdot7H_2O$; pH of 2.8) for 15 weeks also at 423 K. Er and La in the zeolite were subsequently measured by inductively coupled plasma (ICP) mass spectrometry yielding only 656 ppm Er and 195 ppm La, whereas electron-microprobe (EMP) analyses indicated that the Na concentration decreased from originally 8.44 Na pfu to 0.25 Na pfu. The low REE content may be explained by the relatively small free diameter of the channel windows and the large size of hydrated REE ions. The low Na concentration is caused by partial dealumination of the tetrahedral framework where Si replaced some Al of the framework and Al migrated into the structural channel. Dealumination or more generally dissolution phenomena on the crystal surface occurring due to the acidic milieu in the exchange solution were observed as etch pits on scanning-electron microscope (SEM) images.

X-ray single-crystal data of REECl₃-treated heulandite were collected at 100 and 293 K and at 100 K after partial dehydration at 323 and 378 K. Structure refinement using all data sets suggested the presence of low concentrations of octahedrally coordinated Al^{3+} that was dissolved from the framework and incorporated into the channels. T-O distances in the framework, corrected for rotational disorder, are significantly shortened compared with the Na-exchanged precursor heulandite. This indicates that REECl₃-treated heulandite has a significantly lower Al concentration in the framework than the Na-exchanged precursor phase.

INTRODUCTION

Clinoptilolite, $(Na,K)_6[Al_6Si_{30}O_{72}]\cdot20H_2O$, is one of the most abundant and economically important natural zeolites (e.g., Mumpton 1988). However, clinoptilolite crystals are usually small, requiring that single-crystal investigations be made on heulandite, $(Na,K)Ca_4[Al_9Si_{27}O_{72}]\cdot24H_2O$, which has the same framework structure.

The crystal structure of heulandite (space group $C2/m$, $a = 17.70$, $b = 17.94$, $c = 7.42$ Å, and $\beta = 116.40°$; e.g., Gottardi and Galli 1985) contains three types of structural channels confined by tetrahedral ring systems. A and B channels run parallel to the c-axis and are confined by ten- and eight-membered rings, respectively. C channels, confined by another set of eight-membered rings, run parallel to the a-axis and the [102] direction (Merkle and Slaughter 1968; Koyama and Takéuchi 1977). The channels are occupied by cations and H_2O molecules. The structure of untreated heulandite samples was investigated by, e.g., Alberti (1972), Bresciani-Pahor et al. (1980), Alberti and Vezzalini (1983), Hambley and Taylor (1984), and Armbruster and Gunter (1991). Exchange studies on heulandite have recently been performed by Bresciani-Pahor et al. (1981), Gunter et al. (1994), Misaelides et al. (1995), Yang and Armbruster (1996, 1998), Godelitsas et al. (1996a, 1996b), and Stolz and Armbruster (1997).

In the zeolite occurrence at Gibelsbach (Fiesch, Switzerland) the rare-earth elements (REE) distribution between heulandite and accompanying stellerite is significantly different (Armbruster et al. 1996). Stellerite is characterized by a more or less flat REE distribution (chondrite normalized), whereas heulandite is characterized by LREE > HREE. Either these zeolites have a different selectivity for large (LREE) and small (HREE) ions or the zeolites were formed in fluids of different REE^{3+} composition.

Lanthanides are characterized by their high chemical similarity. They occur mostly as trivalent ions. La^{3+} is the largest ion of the lanthanides whereas Er^{3+} is one of the smallest ions of this group (Shannon 1976). Godelitsas et al. (1996a) even conducted exchange experiments with four-valent actinides (e.g., Th^{4+}). Thorium uptake by heulandite was especially favored in solutions with low Th concentrations. However, thorium precipitated mainly on the heulandite surface and did not appear to occupy the structural channels (Godelitsas et al. 1996a).

High concentrations of REE^{3+} in solution require acidic pH-conditions unless a complexing agent is used. Thus, in addition to REE^{3+}, also protons or more generally H_3O^+ ions may compete to occupy extraframework positions in the channels. The chemical behavior of natural zeolites in an acidic aqueous solution is of environmental, geochemical and technological

---

*E-mail: armbruster@krist.unibe.ch

significance. At low pH, zeolites may interact with oxonium (H_3O^+) ions and certain physicochemical phenomena such as hydrolysis of the solids, degradation, dissolution, incorporation of oxonium and even phase transformations may occur. The atomic-force microscope (AFM) images by Yamamoto et al. (1996) of heulandite in acidic aqueous solution showed that 0.1 M H_2SO_4 attacked the (010) surface of heulandite, forming etch pits and the topmost aluminosilicate layers were removed in a layer-by-layer process. Completely dealuminated heulandite crystals were observed after treatment in HCl solutions (Misaelides et al. 1996). Tsitsishivili (1978) showed that heulandite in 1 M hydrochloric acid loses significant amounts of framework Al and extraframework cations of the channels whereas only a negligible amount of Si is extracted. Filippidis et al. (1996) report acid resistance of heulandite due to its high Si content compared with natrolite and thomsonite.

This study investigates the incorporation of REE, in particular La and Er, into heulandite and possible interactions of the zeolite with acidic aqueous solutions.

EXPERIMENTAL METHODS

Single crystals of natural heulandite $Na_{0.96}Ca_{3.54}K_{0.09}$ $[Al_{8.62}Si_{27.51}O_{72}] \cdot nH_2O$ (Yang and Armbruster 1996) from Nasik, India (Sukheswala et al. 1974), were broken to 0.1–0.5 mm samples that were placed in a Teflon autoclave filled with 4 M NaCl solution. The exchange reaction was run for 12 weeks at 423 K yielding an almost fully Na-exchanged heulandite as a precursor phase. The exchange products were qualitatively analyzed with a scanning electron microscope (SEM) every four weeks during the exchange. Subsequently, about 2 g of the Na-exchanged heulandite were equilibrated at 423 K in 0.5 M REE solution (120 mL), consisting of 0.25 M $ErCl_3 \cdot 6H_2O$ and 0.25 M $LaCl_3 \cdot 7H_2O$ with 3 mL of 25% HCl added to increase the solubility of the REE chlorides. The experiment lasted 15 weeks, the solution was changed after one, two, four, and six weeks. The exchange reaction of the heulandite was qualitatively monitored by energy-dispersive analyses using a scanning electron microscope (SEM).

The pH of the exchange solution was analyzed with an ORION digital pH meter (Model 720A) calibrated with two buffer solutions of pH 4.00 and 7.00. A pH of 2.8 was recorded for the starting solution without the heulandite sample and 4.67 at the end of the experiment after a total of 15 weeks, nine weeks after the last solution exchange.

The quantitative chemical composition of the exchange product was determined with a CAMECA SX50 electron microprobe (EMP) operating at 15 kV and 10 nA beam current and a defocused beam diameter of about 20 μm to minimize sample destruction. Measuring time was 20 s on the peaks and 10 s on the background. The following natural and synthetic minerals were used as standards: albite (Na), adularia (K, Si), fluorapatite (P), spinel (Mg), anorthite (Ca, Al), almandine (Fe), tephroite (Mn), $La_{0.95}Nd_{0.05}TiO_3$ (La), and ErF_3 (Er). The detection limit of the EMP for low concentrations of REE is about 0.1 wt%.

A total of 12.8 mg of heulandite was separated after 15 weeks treatment in 0.5 M REE solution at 423 K, dissolved in 95% HF, evaporated and subsequently redissolved in KNO_3. The La and Er contents of the sample were quantitatively measured by inductively coupled plasma (ICP) mass spectrometry.

The crystal structure of the exchanged products was studied by single-crystal X-ray diffraction on an Enraf-Nonius CAD4 diffractometer (graphite-monochromatized Mo$K\alpha$ X-radiation) at room temperature (REE293), at 100 K (REE100), at 100 K after heating to 323 K for 2 hours (DEHY323), and finally at 100 K after heating to 323 K for 2 hours and to 378 K for 2 hours (DEHY378). Heating and subsequent quenching to 100 K was done directly on the single-crystal diffractometer by a temperature-controlled nitrogen stream. Two crystals, both ca. 0.25 mm × 0.25 mm × 0.1 mm in dimension, were used for the X-ray experiments. The crystal of the REE293 measurement was lost, and a second crystal was used for the remaining three experiments. The use of two different crystals from the same batch, leading to similar results, also confirms the validity of the findings. Data reduction, including background and Lorentz-polarization corrections and an empirical absorption correction based on ψ-scans, was performed using the SDP (Enraf-Nonius 1983) program library. The program SHELXTL (Siemens 1994) was used for structure refinement in space group $C2/m$. Analyses of difference Fourier syntheses led to the positions of channel ions and molecules. In general, atom positions were assigned according to electron-density maxima and reasonable distances and bond angles to neighboring atoms and H_2O molecules. The refinements were performed with anisotropic displacement parameters for framework atoms. In addition, the populations of channel H_2O were allowed to vary but if the isotropic displacement parameter exceeded $U_{iso} > 0.20$, it was fixed at $U_{iso} = 0.20$ Å^2. In addition, in DEHY323 and DEHY378 the channel Al3 displacement parameter was fixed at $U_{iso} = 0.03$ Å^2. Experimental details of data collections and structure refinements are summarized in Table 1.

RESULTS

Electron microprobe analyses of the Na-exchanged precursor phase gave an average composition of $Na_{8.44}Ca_{0.09}K_{0.01}$ $[Al_{8.63}Si_{27.37}O_{72}] \cdot nH_2O$ with Al varying between 8.26 and 8.96 pfu. This variation conforms with the composition of the natural starting material for which values between $Na_{0.81}Ca_{3.46}K_{0.12}$ $[Al_{8.26}Si_{27.74}O_{71.80}] \cdot nH_2O$ and $Na_{1.07}Ca_{3.61}K_{0.13}[Al_{8.96}Si_{27.04}O_{71.72}]$ $\cdot nH_2O$ were found. Corresponding analyses of the REE-treated heulandite (15 weeks in 0.5 M REE solution) indicated that the La or Er contents in heulandite were below the detection limit. The ICP analyses yielded 195 ppm La and 656 ppm Er. Surprisingly, the Na content of the heulandite was drastically reduced to 0.25 Na pfu during the exchange process compared with the starting material with 8.44 Na pfu. The average composition of the REE-treated heulandite, obtained from several EMP point analyses, was calculated corresponding to two models: (1) Normalization to Al + Si = 36 and oxygen fixed at 72 pfu yielded $H_{8.53}Na_{0.25}K_{0.02}Ca_{0.02}[Al_{8.84}Si_{27.16}O_{72}] \cdot nH_2O$ where H was calculated to compensate for the overall charge deficit (minimum and maximum Al pfu were 8.45 and 9.21, respectively). An uptake of H^+, or more generally H_3O^+ in aqueous solution, is also suggested by the low pH of 2.8 of the starting REE solution. (2) Normalization to 72 O pfu yielded $Na_{0.27}K_{0.02}Ca_{0.02}Al_{2.27}[Al_{7.13}Si_{28.87}O_{72}]$ where excess Al relative to Si + Al = 36 was assumed as channel cation.

TABLE 1. Data collection and refinement parameters for REE-treated heulandites (REE293, REE100, DEHY323, and DEHY378)

	REE293	REE100	DEHY323	DEHY378
conditions	293 K	100 K	100 K after heating to 323 K for 2 hours	100 K after heating to 323 K for 2 h and 373 K for 2 h
space group	$C2/m$	$C2/m$	$C2/m$	$C2/m$
a (Å)	17.649(6)	17.611(6)	17.583(6)	17.608(4)
b (Å)	17.980(5)	17.933(5)	17.695(5)	17.656(5)
c (Å)	7.412(2)	7.398(2)	7.408(2)	7.414(2)
β (°)	116.22(3)	116.29(3)	116.52(3)	116.42(2)
θ max. (°)	30	30	25	25
hkl (min., max.)	$-24 < h < 23$, $-1 < k < 25$, $-1 < l < 10$	$-24 < h < 23$, $-1 < k < 25$, $-1 < l < 7$	$-20 < h < 19$, $-1 < k < 20$, $-1 < l < 8$	$-20 < h < 18$, $0 < k < 20$, $0 < l < 7$
scan type	$2.0°\ \omega + 0.35\ \tan\theta$	$1.5°\ \omega + 0.35\ \tan\theta$	$1.5°\ \omega + 0.35\ \tan\theta$	$1.5°\ \omega + 0.35\ \tan\theta$
measured reflections	4060	3562	2501	1873
unique reflections	3173	2712	1880	1722
R_{int} (%)	2.61	1.20	1.05	0.87
obs. reflect. [I > 2σ(I)]	1884	2117	1556	1424
$R1$ (%)	4.54	4.79	4.33	4.03
$wR2$ (%)	11.56	13.67	13.09	11.60
GooF	0.999	1.011	1.04	1.025
H_2O sites lost			WA2, WA5, WB1, WBb	WA8
H_2O sites gained				WC33, WC4

Notes: $R1 = (\Sigma||F_o|-|F_c||)/(\Sigma|F_o|)$; $wR2 = \{[\Sigma(F_o^2-F_c^2)^2]/[\Sigma w(F_o^2)^2]\}^{1/2}$; GooF $= \{[\Sigma w(F_o^2-F_c^2)^2]/(n-p)\}^{1/2}$.

TABLE 2a. Atomic positional parameters and B_{eq} (Å^2) values with standard deviations in parentheses for heulandite REE293

Atom	Population	x/a	y/b	z/c	B_{eq} (Å^2)
T1		0.17734(6)	0.32961(7)	0.0917(2)	1.61(2)
T2		0.28418(7)	0.41088(7)	0.4894(2)	1.89(2)
T3		0.29145(7)	0.19068(7)	0.2853(2)	1.63(2)
T4		0.43161(7)	0.29831(7)	0.5786(2)	1.72(2)
T5		0	0.2771(1)	0	1.82(3)
O1		0.2985(3)	0.5	0.5263(8)	3.10(9)
O2		0.2644(3)	0.1219(2)	0.3841(6)	3.42(7)
O3		0.3131(3)	0.1556(2)	0.1120(5)	3.42(7)
O4		0.2253(2)	0.3965(2)	0.2459(5)	3.22(6)
O5		0.5	0.3208(3)	0.5	3.9(1)
O6		0.0785(2)	0.3327(2)	0.0409(5)	3.05(7)
O7		0.3755(3)	0.2295(2)	0.4533(6)	4.35(7)
O8		0.0179(2)	0.2246(2)	0.1894(5)	3.70(7)
O9		0.2150(2)	0.2501(2)	0.1882(5)	3.10(6)
O10		0.3765(2)	0.3711(2)	0.5591(6)	3.70(7)
Al1	0.120(9)	0	0.4221(8)	0	1.7(4)
Al2	0.13(1)	0.488(1)	0	0.556(3)	3.6(5)
Al3	0.08(1)	0.205(2)	0.5	0.199(4)	3.0(8)
NaB	0.39(2)	0.468(1)	0.5	0.771(3)	11.0(8)
WA1	0.51(5)	0.369(1)	0	0.348(4)	8.4(9)
WA2	0.28(3)	0.390(4)	0	0.51(1)	15.79*
WA3	0.39(3)	0.402(3)	0	0.235(9)	15.79*
WA4	0.17(3)	0.398(3)	0	0.061(9)	6.5(19)
WA5	0.47(6)	0.433(2)	0	0.788(8)	15.0(21)
WA6	0.47(5)	0.560(2)	0	0.036(7)	13.9(18)
WA8	0.37(3)	0.496(2)	0.091(1)	0.583(4)	11.9(12)
WA9	0.27(3)	0.478(2)	0.072(2)	0.707(6)	11.3(16)
WB1	0.39(3)	0.393(2)	0.411(2)	0.097(5)	13.8(14)
WBb	0.47(2)	0.436(2)	0.430(2)	0.001(4)	15.79*
WB2	0.55(3)	0.512(2)	0.5	0.564(3)	11.1(9)
WB3	0.14(2)	0.406(3)	0.5	0.059(6)	3.7(12)
WC2	0.64(4)	0.212(2)	0	−0.014(4)	9.5(7)
WC3	0.52(3)	0.2582(8)	0	0.089(2)	3.0(3)

Note: Starred atoms were refined with fixed isotropic displacement parameters. Anisotropically refined atoms are given in the form of the isotropic equivalent displacement parameter defined as $B_{eq} = 8/3\ \pi^2\ \Sigma_i[\Sigma_j(U_{ij}\ a_i^* a_j^* a_i a_j)]$.

Many degraded crystals with etch pits, observed on SEM images of the exchange product, led to the assumption of acid-attacked crystal surfaces, since the surface of the starting material (Na-exchanged heulandite) was intact. The surface erosion was interpreted in terms of a dealumination process due to the low pH (2.8) of the solution (e.g., Yamamoto et al. 1996).

Four single-crystal X-ray data sets were collected on differently treated crystals, two in hydrated state, and two partially dehydrated. Atomic coordinates and site populations are in Table 2 and atomic displacement parameters are in Table 3[1].

All four refined structures have a very similar framework. The Si/Al tetrahedral distribution is highly disordered, indi-

[1]For a copy of Table 3, Document AM-99-014, contact the Business Office of the Mineralogical Society of America (see inside front cover of recent issue) for price information. Deposit items may also be available on the American Mineralogist web site at http://www.minsocam.org or current web address.

TABLE 2b. Atomic positional parameters and B_{eq} (Å^2) values with standard deviations in parentheses for heulandite REE100

Atom	Population	x/a	y/b	z/c	B_{eq} (Å^2)
T1		0.17760(5)	0.33000(6)	0.0926(2)	1.46(2)
T2		0.28447(6)	0.41110(6)	0.4904(2)	1.77(2)
T3		0.29189(6)	0.19069(5)	0.2854(2)	1.45(1)
T4		0.43213(6)	0.29855(6)	0.5794(2)	1.62(2)
T5		0	0.27754(9)	0	1.76(2)
O1		0.2988(3)	0.5	0.5280(8)	3.00(8)
O2		0.2652(2)	0.1218(2)	0.3846(5)	3.29(6)
O3		0.1863(2)	0.3447(2)	-0.1126(5)	3.28(7)
O4		0.2267(2)	0.3971(2)	0.2460(5)	3.22(6)
O5		0.5	0.3227(3)	0.5	4.1(1)
O6		0.0789(2)	0.3336(2)	0.0451(5)	2.93(6)
O7		0.3760(2)	0.2298(2)	0.4535(5)	4.30(7)
O8		0.4839(2)	0.2752(2)	0.8118(5)	3.72(7)
O9		0.2153(2)	0.2498(2)	0.1891(5)	2.67(5)
O10		0.3767(2)	0.3710(2)	0.5630(6)	3.71(7)
Al1	0.119(9)	0	0.4225(7)	0	1.6(3)
Al2	0.109(9)	0.489(1)	0	0.550(2)	2.2(4)
Al3	0.074(9)	0.203(1)	0.5	0.200(4)	2.2(6)
NaB	0.38(2)	0.466(1)	0.5	0.767(3)	10.1(7)
WA1	0.56(3)	0.373(1)	0	0.369(3)	8.1(7)
WA2	0.15(3)	0.444(8)	0	0.62(2)	15.79*
WA3	0.43(3)	0.400(3)	0	0.242(8)	15.79*
WA4	0.15(3)	0.395(3)	0	0.067(7)	4.4(13)
WA5	0.49(5)	0.440(2)	0	0.812(7)	12.7(15)
WA6	0.41(5)	0.563(2)	0	0.025(7)	12.5(17)
WA8	0.35(2)	0.496(2)	0.091(1)	0.591(4)	10.42(8)
WA9	0.16(1)	0.476(2)	0.076(1)	0.716(4)	4.7(8)
WB1	0.31(3)	0.395(2)	0.411(2)	0.105(5)	13.0(17)
WBb	0.46(2)	0.433(2)	0.430(2)	0.006(4)	15.79*
WB2	0.55(3)	0.511(2)	0.5	0.561(3)	10.1(8)
WB3	0.12(8)	0.409(2)	0.5	0.076(5)	2.3(8)
WC2	0.65(4)	0.215(1)	0	-0.008(3)	8.0(6)
WC3	0.39(3)	0.258(1)	0	0.085(2)	3.0(4)

Note: Starred atoms were refined with fixed isotropic displacement parameters. Anisotropically refined atoms are given in the form of the isotropic equivalent displacement parameter defined as $B_{eq} = 8/3 \pi^2 \Sigma_i[\Sigma_j(U_{ij} a_i^* a_j^* a_i a_j)]$.

TABLE 2c. Atomic positional parameters and B_{eq} (Å^2) values with standard deviations in parentheses for heulandite DEHY323

Atom	Population	x/a	y/b	z/c	B_{eq} (Å^2)
T1		0.17822(6)	0.33236(7)	0.0912(2)	1.80(2)
T2		0.28602(7)	0.41093(7)	0.4940(2)	2.07(2)
T3		0.29190(7)	0.19000(7)	0.2828(2)	1.82(2)
T4		0.43360(7)	0.29733(7)	0.5820(2)	1.91(2)
T5		0	0.2813 (1)	0	2.05(3)
O1		0.3019(4)	0.5	0.5391(9)	3.9(1)
O2		0.2645(3)	0.1217(2)	0.3843(6)	4.43(8)
O3		0.3144(2)	0.1508(2)	0.1146(5)	3.65(7)
O4		0.2304(2)	0.3977(2)	0.2497(5)	3.50(7)
O5		0.5	0.3217(4)	0.5	5.2(1)
O6		0.0799(2)	0.3374(2)	0.0499(5)	2.86(6)
O7		0.3757(3)	0.2298(3)	0.4517(6)	5.17(8)
O8		0.0141(2)	0.2284(2)	0.1878(5)	4.03(8)
O9		0.2153(2)	0.2497(2)	0.1797(5)	2.93(6)
O10		0.3792(2)	0.3713(2)	0.5719(6)	4.26(8)
Al1	0.12(1)	0	0.4210(9)	0	2.1(5)
Al2	0.13(1)	0.489(1)	0	0.550(3)	3.7(5)
Al3	0.033(5)	0.235(4)	0.5	0.178(9)	2.37*
NaB	0.19(2)	0.462(2)	0.5	0.724(4)	8.01(4)
WA1	0.12(3)	0.373(4)	0	0.38(1)	4.9(19)
WA3	0.12(3)	0.391(3)	0	0.296(9)	4.1(16)
WA4	0.12(4)	0.418(7)	0	0.10(2)	12.2(52)
WA6	0.25(3)	0.076(2)	0.5	0.047(5)	5.92(4)
WA8	0.10(1)	0.505(3)	0.089(3)	0.620(7)	5.5(16)
WA9	0.15(1)	0.473(2)	0.080(2)	0.710(4)	4.7(9)
WB2	0.32(2)	0.525(4)	0.5	0.612(7)	15.79*
WB3	0.17(2)	0.410(2)	0.5	0.079(4)	2.3(7)
WC2	0.30(5)	0.224(3)	0	0.034(5)	4.2(7)
WC3	0.22(5)	0.259(3)	0	0.083(5)	2.9(9)

Note: Starred atoms were refined with fixed isotropic displacement parameters. Anisotropically refined atoms are given in the form of the isotropic equivalent displacement parameter defined as $B_{eq} = 8/3 \pi^2 \Sigma_i[\Sigma_j(U_{ij} a_i^* a_j^* a_i a_j)]$.

TABLE 2d. Atomic positional parameters and B_{eq} (Å^2) values with standard deviations in parentheses for heulandite DEHY378

Atom	Population	x/a	y/b	z/c	B_{eq} (Å^2)
T1		0.17810(6)	0.33296(7)	0.0907(2)	2.06(2)
T2		0.28613(7)	0.41108(7)	0.4939(2)	2.25(2)
T3		0.29161(7)	0.18976(7)	0.2820(2)	2.13(2)
T4		0.06675(7)	0.20343(7)	0.4196(2)	2.15(2)
T5		0	0.2810(1)	0	2.22(3)
O1		0.3022(4)	0.5	0.5402(8)	4.3(1)
O2		0.2628(3)	0.1220(3)	0.3823(7)	5.07(9)
O3		0.3126(2)	0.1494(2)	0.1124(5)	3.80(7)
O4		0.2285(2)	0.3996(2)	0.2485(5)	3.81(7)
O5		0	0.1788(4)	0.5	5.9(2)
O6		0.0795(2)	0.3370(2)	0.0462(5)	3.16(7)
O7		0.1238(3)	0.2721(3)	0.5499(6)	5.47(8)
O8		0.0160(2)	0.2280(2)	0.1892(5)	4.46(8)
O9		0.2164(2)	0.2510(2)	0.1809(5)	3.34(6)
O10		0.1220(2)	0.1297(2)	0.4358(6)	4.63(8)
Al1	0.10(1)	0	0.421(1)	0	2.6(6)
Al2	0.08(1)	0.490(2)	0	0.555(4)	3.5(8)
Al3	0.026(5)	0.229(5)	0.5	0.18(1)	2.37*
NaB	0.13(3)	0.481(4)	0.5	0.66(1)	14.0(33)
WA1	0.10(3)	0.371(5)	0	0.37(1)	5.8(25)
WA3	0.03(2)	0.392(5)	0	0.31(2)	0.1(31)
WA4	0.10(3)	0.410(6)	0	0.12(2)	9.8(41)
WA6	0.18(2)	0.073(2)	0.5	0.049(6)	5.2(12)
WA9	0.14(1)	0.479(2)	0.081(2)	0.696(6)	6.7(14)
WB2	0.16(4)	0.5	0.5	0.5	15.79 *
WB3	0.09(2)	0.411(2)	0.5	0.083(6)	1.8(12)
WC2	0.18(4)	0.232(3)	0	0.049(5)	1.2(9)
WC4	0.17(3)	0.284(3)	0	0.23(1)	4.7(12)
WC3	0.26(3)	0.266(3)	0	0.10(1)	3.95 *
WC33	0.08(3)	0.231(4)	0.5	-0.01(1)	2.2(18)

Note: Starred atoms were refined with fixed isotropic displacement parameters. Anisotropically refined atoms are given in the form of the isotropic equivalent displacement parameter defined as $B_{eq} = 8/3 \; \pi^2 \; \Sigma_i[\Sigma_j(U_{ij} \; a_i^* \; a_j^* \; a_i \cdot a_j)]$.

cated by the T-O distances (Table 4). Most of the framework Al is on the T2 site that exhibited the longest T-O distances, whereas the Si/Al distribution among the other tetrahedral sites is fairly even. Average T2-O distances became significantly shorter upon partial dehydration and T and O displacement parameters increased. In particular, O displacement parameters were strongly anisotropic and showed significant elongation perpendicular to the T-O vectors. This type of anisotropy is characteristic of rotational disorder. Applying a corresponding correction according to the riding model of Johnson (1970) (Table 4) individual T-O distances, among the differently treated samples, became identical within one standard deviation. A corresponding riding model was also applied on T-O distances of the Na-exchanged percursor phase (Yang and Armbruster 1996). The riding motion model for SiO$_4$ tetrahedra is based on the hypothesis that O has all of the translational motion of Si plus an additional motion uncorrelated with the instantanous position of Si (Johnson 1970).

A low-occupancy Na position was located in the B channel for all structures but Na is most probably disordered with a volatile species (H$_2$O or H$_3$O$^+$). With increasing degree of dehydration, the population of the Na site decreased from 0.39 to 0.19, and then to 0.13. Thus the Na site must be partially occupied by H$_2$O or H$_3$O$^+$. The most dehydrated sample (DEHY378) still exhibits a Na population corresponding to 0.5 pfu indicating that even in this dehydrated variety the population is a mixture of Na and (H$_2$O, H$_3$O$^+$) because only 0.25 Na pfu were analyzed by EMP. Na-O bond lengths are in Table 4.

The occurrence of strikingly well-defined electron-density peaks within a distance of ca. 2 Å from framework oxygen sites, positioned in the structural channels, suggests the presence of small cations, though with low populations. The observed peak-O distance of ca. <2 Å excludes an interpretation in terms of channel Er^{3+} or La^{3+} because those ions would have REE^{3+}-O distances of >2.3 Å (Shannon 1976). Even longer framework oxygen distances (Lundgren and Taesler 1979) would be expected for oxonium ions (H$_3$O$^+$). The etch pits on SEM images and the short T-O distances as indirect evidence for surface dealumination further strongly suggest that the observed additional electron densities are caused by dissolved Al^{3+}, which was subsequently incorporated into the structural channels.

Bond lengths of re-incorporated channel aluminum to framework oxygen and channel H$_2$O are in Table 5. The populations of Al atoms incorporated into the channels are very low. The total population of all channel Al sites yields a maximum amount of Al(channel) = 1.32 pfu. Most of the octahedrally coordinated channel Al (Al1 and Al2) was closest to the Si-rich T5 tetrahedra and only the low-populated Al3 site was close to the Al-rich tetrahedra T2. The populations of H$_2$O decreased drastically with heating (DEHY323 and DEHY378), and several H$_2$O sites in the B channel disappeared (Figs. 1 and 2). The most pronounced change of unit-cell dimensions upon dehydration was observed for b, decreasing from 17.933(5) Å for REE100 to 17.656(5) Å for DEHYD378. Follow H$_2$O concentrations (pfu) were refined: 28.6 (REE293), 25.8 (REE100), 17.7 (DEHY323), and 15.1 (DEHY378). The following nomenclature for channel H$_2$O sites is used: W stands for H$_2$O molecules, followed by A, B, or C depending on the channel type.

DISCUSSION

All data sets were refined in space group $C2/m$ converging at R-values of 4.54% (REE293), 4.79% (REE100), 4.33%

TABLE 4. T-O and Na-O distances (Å) in REE-treated heulandite. T-O distances corrected for rotational disorder (Johnson 1970) are in parentheses

	REE293	REE100	DEHY323	DEHY378	Na-Heul*
T1-O9	1.607(3) (1.624)	1.612(3) (1.627)	1.615(3) (1.629)	1.610(3) (1.625)	1.634(2) (1.643)
T1-O3	1.615(3) (1.635)	1.615(3) (1.636)	1.616(3) (1.636)	1.615(4) (1.635)	1.629(2) (1.644)
T1-O6	1.615(2) (1.632)	1.615(3) (1.631)	1.616(3) (1.628)	1.619(3) (1.631)	1.644(1) (1.651)
T1-O4	1.616(3) (1.635)	1.616(3) (1.635)	1.611(3) (1.629)	1.619(3) (1.638)	1.628(2) (1.640)
average	1.613 (1.632)	1.614 (1.632)	1.614 (1.631)	1.616 (1.632)	1.634 (1.645)
T2-O1	1.626(1) (1.640)	1.619(1) (1.633)	1.610(1) (1.631)	1.604(1) (1.626)	1.642(1) (1.654)
T2-O2	1.635(3) (1.653)	1.639(3) (1.657)	1.627(4) (1.655)	1.621(4) (1.655)	1.664(1) (1.674)
T2-O10	1.640(2) (1.662)	1.634(3) (1.657)	1.632(3) (1.657)	1.631(3) (1.658)	1.665(1) (1.676)
T2-O4	1.656(3) (1.672)	1.656(3) (1.673)	1.647(3) (1.664)	1.655(3) (1.672)	1.670(1) (1.680)
average	1.639 (1.657)	1.636 (1.655)	1.629 (1.652)	1.628 (1.653)	1.660 (1.671)
T3-O2	1.614(3) (1.634)	1.609(3) (1.629)	1.606(3) (1.635)	1.606(4) (1.639)	1.632(2) (1.643)
T3-O7	1.615(3) (1.646)	1.613(3) (1.646)	1.611(4) (1.649)	1.605(4) (1.643)	1.622(2) (1.644)
T3-O9	1.617(3) (1.635)	1.612(3) (1.628)	1.611(3) (1.625)	1.613(3) (1.627)	1.635(2) (1.644)
T3-O3	1.621(3) (1.641)	1.617(3) (1.639)	1.621(3) (1.641)	1.625(3) (1.642)	1.633(2) (1.649)
average	1.617 (1.639)	1.613 (1.636)	1.612 (1.638)	1.612 (1.638)	1.631 (1.645)
T4-O10	1.598(3) (1.621)	1.599(3) (1.624)	1.605(4) (1.631)	1.597(4) (1.624)	1.627(2) (1.637)
T4-O7	1.599(4) (1.630)	1.596(3) (1.628)	1.584(4) (1.622)	1.595(4) (1.633)	1.610(2) (1.632)
T4-O8	1.603(3) (1.625)	1.604(3) (1.628)	1.600(3) (1.624)	1.593(5) (1.618)	1.627(2) (1.641)
T4-O5	1.606(2) (1.632)	1.608(2) (1.635)	1.598(2) (1.637)	1.599(2) (1.641)	1.630(1) (1.645)
average	1.602 (1.627)	1.602 (1.629)	1.597 (1.629)	1.596 (1.629)	1.624 (1.639)
T5-O8 ×2	1.602(3) (1.624)	1.603(3) (1.626)	1.601(3) (1.623)	1.607(4) (1.632)	1.618(2) (1.633)
T5-O6 ×2	1.625(2) (1.639)	1.626(3) (1.639)	1.623(3) (1.633)	1.620(3) (1.631)	1.629(1) (1.636)
average	1.614 (1.632)	1.615 (1.633)	1.612 (1.628)	1.614 (1.632)	1.624 (1.635)
NaB-O1	2.72(1)	2.67(1)	2.52(2)	2.85(4)	2.54(1)
NaB-O10 ×2	2.86(1)	2.82(1)	2.67(1)	2.80(3)	2.44(2)/2.89(2)
NaB-WB2	2.67(2)	2.63(2)	2.62(5)	–	
NaB-WB1 ×2	2.71(2)	2.72(3)	–	–	
NaB-WB3	2.81(3)	2.89(3)	3.14(3)	–	

*Yang and Armbruster (1996): Na-exchanged heulandite at 100 K.

TABLE 5. Distances (Å) within Al^{3+}-octahedra of re-incorporated Al^{3+} in the channels of heulandite

Distances (Å)	REE293	REE100	DEHY323	DEHY378
Al1-O6 ×2	2.05(1)	2.04(1)	1.96(1)	1.96(1)
Al1-WA6 ×2	1.70(1)	1.75(1)	1.85(2)	1.84(2)
Al1-WA9 ×2	2.01(3)	1.94(2)	1.99(3)	2.13(3)
Al2-WA1	1.98(2)/2.29(2)	1.90(2)/2.23(1)	1.86(4)/2.28(3)	1.93(8)/2.26(5)
Al2-WA3	1.85(5)/2.16(6)	1.86(5)/2.11(6)	1.87(4)/1.89(3)	1.89(8)/1.89(5)
Al2-WA8 ×2	2.02(2)	2.01(2)	2.03(5)	–
Al2-WA9 ×2	1.82(3)	1.93(2)	1.93(3)	1.82(3)
Al3-O1	2.26(2)	2.26(2)	2.35(6)	2.46(8)
Al3-O4 ×2	1.90(1)	1.89(1)	1.89(1)	1.86(2)
Al3-WA4	1.97(5)	1.97(4)	2.6(1)	2.4(1)
Al3-WA5	2.50(2)	2.47(2)	–	–
Al3-WA6	2.28(3)	2.21(3)	2.54(4)	2.41(5)
Al3-WC2	2.42(2)	2.42(2)	2.03(6)	2.08(7)
Al3-WC3	2.51(2)	2.49(2)	2.00(6)	2.03(9)

(DEHY323), 4.03% (DEHY378). These values are slightly higher than those for exchanged heulandites in previous studies (e.g., Gunter et al. 1994; Yang and Armbruster 1996), consistent with rather strong disorder within the tetrahedral framework and of channel occupants. Furthermore, the absence of large stabilizing cations in the channels causes a distortion of the tetrahedral framework which can be deduced from the high B_{eq} values of T and O, given in Table 2. The B_{eq} values increased with dehydration and were highest for the sample DEHY378. REE100 reveals slightly lower displacement parameters than REE293 due to low temperature reducing dynamic disorder. Rotational disorder of TO$_4$ groups leads to apparent shortening of T-O distances. After a correction for tetrahedral rotation ac-

cording to Johnson (1970) the apparent T-O distances increased by ca. 0.01 Å, but the average mean T-O distances remained 0.01 Å shorter for REE-treated heulandite (Table 4) compared with Na-exchanged heulandite reported by Yang and Armbruster (1996). The most Al-enriched tetrahedron, T2, exhibits a mean T-O distance 0.016 Å shorter than in the Na-exchanged reference heulandite. This implies a decreased Al concentration in the framework due to partial dealumination in acid-treated heulandite. This is also confirmed by other studies, e.g., Kerr (1969) observed channel Al in protonated zeolite Y (faujasite structure) and Kolodziejski et al. (1993) found by NMR spectroscopy that four-coordinated framework Al was removed from the zeolite Y framework and transformed into six-coordinated
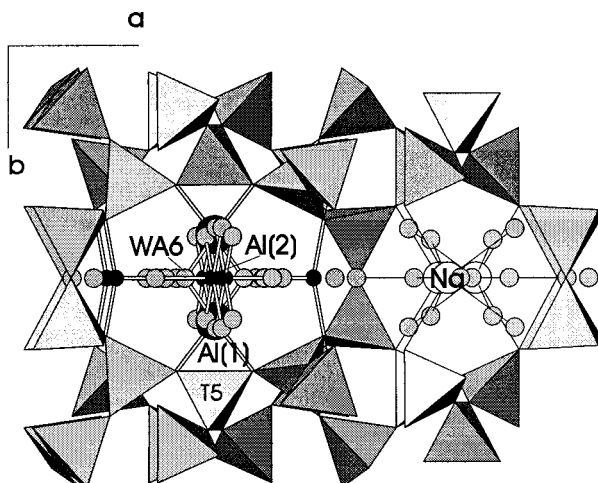
FIGURE 1. Portion of the heulandite structure according to the REE100 refinement displaying the ten-membered ring confining the A channel and the eight-membered ring confining the B channel. Partially occupied Na in the B channel is displayed as white sphere with single-line bonds to framework oxygen and H$_2$O molecules (small gray spheres). Low occupied Al sites in the A channel are shown as black spheres with double-line bonds to coordinating framework oxygen atoms and H$_2$O molecules. The Al1 octahedron is edge-sharing with the framework T5 tetrahedron. The Al2 octahedron forms a disordered [Al(H$_2$O)$_6$]$^{3+}$ complex in the center of the A channel.
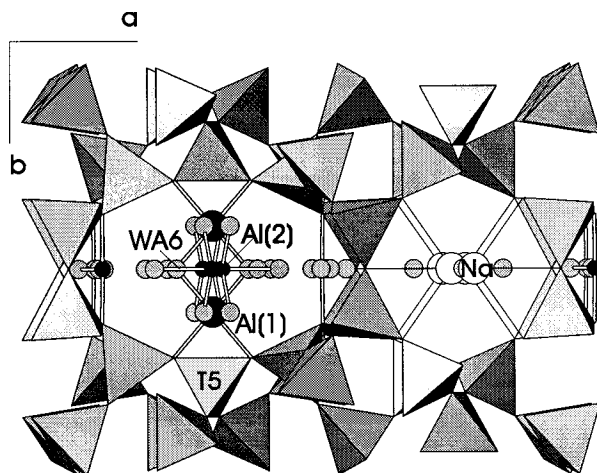
FIGURE 2. Portion of the heulandite structure according to the DEHY378 refinement (sample dehydrated 2 h at 323 and 378 K, respectively, and subsequently quenched to 100 K). Symbols as in Figure 1. Some H$_2$O sites have vanished in the B channel. H$_2$O and/or H$_3$O$^+$ sites have significantly lower occupancies than those in the REE100 refinement.

channel Al(H$_2$O)$_6^{3+}$ and Al(Cl$^-$)(H$_2$O)$_5^{2+}$. The acidic milieu of the solution provokes dealumination of heulandite (Yamamoto et al. 1996; Godelitsas et al. 1996a; Misaelides et al. 1996; Filippidis et al. 1996). The attacked surface can be observed in form of degraded crystals with etch pits in SEM images.

Test structure-refinements, performed in this study, allowing the T populations to vary yielded always complete occupancy. Thus we must assume that Si replaced tetrahedral Al where Si was supplied from dissolved heulandite layers. The replaced tetrahedral Al, however, is not expelled from the structure but forms octahedral coordination by H$_2$O and/or framework oxygen within the structural cavities. Since most of the Al remains in the structure, electron-microprobe analyses are not very sensitive on this type of framework dealumination. Furthermore, the slight variation of the Si/Al ratio in the starting heulandite precludes an unmistakable interpretation of this ratio after REE-treatment.

The low-occupancy Na site exhibits the expected distances to framework O atoms of 2.5–2.9 Å. The refined NaB position is in good agreement with the Na position in the B channel refined by Gunter et al. (1994) and Yang and Armbruster (1996). The apparent decreasing population of Na with dehydration is due to a mixed occupancy of Na and probably H$_3$O$^+$ (oxonium). The latter is partly expelled or rearranged upon heating. The Na to framework-oxygen distance (Table 4) appears too short for mixed Na and H$_2$O occupancy. Lundgren and Taesler (1979) give an average OH⋯O distance of 2.59 Å for oxonium which agrees better with the observed distances. Furthermore, oxonium is well established in crystalline hydrates of strong acids (Lundgren and Taesler 1979) and could also balance the defi-

cient cation charges in the channels of heulandite.

Godelitsas et al. (1996a) suggested H$^+$ adsorption by the zeolite replacing Na$^+$ through ion-exchange reactions and bonding H$^+$ to convenient Lewis base sites of the zeolite structure. However, especially for highly hydrated heulandite in aqueous solution, H$_3$O$^+$ within the structural channels instead of H$^+$ must also be considered.

Three independent observations are available to derive a crystal chemical formula for REE-treated heulandite: (1) the electron-microprobe analyses; (2) T-O distances with information on the Si/Al ratio in the framework; (3) population refinements of channel Al. In particular, the Si/Al ratio derived from T-O distances and the refined concentration of channel Al are associated with large errors. Individual T-O distances are accompanied by errors of ca. 0.003 Å (Table 4) thus the systematic decrease by 0.01 Å relative to Na-exchanged heulandite will have a similar error. Furthermore, Alberti et al. (1990) used more sophisticated models (taking into account the influence of bonding forces and Si,Al disorder on T-O distances) than only T-O distances to estimate the Al distribution in heulandites and clinoptilolites but their mean Al estimate still deviated by more than 2% from the chemical composition. Channel Al is easily identified by its short Al-O distance if Al is close to a framework oxygen. However, if an Al(H$_2$O)$_6^{3+}$ complex is disordered in the center of a structural cavity it is easily overlooked or misinterpreted.

If 1.3 Al pfu (as refined) are positioned in the structural cavities, then the electron-microprobe analyses normalized to Al^{IV} + Si = 36 and O = 72 yield the formula H$_{3.63}$Na$_{0.27}$K$_{0.02}$Ca$_{0.02}$ Al$_{1.3}$[Al$_{7.86}$Si$_{28.14}$O$_{72}$]·nH$_2$O. Alternatively, a decrease of average

T-O distances by 0.01 Å, relative to Na-exchanged heulandite, suggests that in REE-treated heulandite the framework Al concentration is lowered by ca. 6% which leads to a framework composition of $[Al_{6.63}Si_{29.37}O_{72}]^{6.63-}$. However, electron-microprobe analyses require that additional 2.93 Al^{3+} pfu must be considered as channel cations which exceeds the number of positive charges for neutrality. Thus the limiting composition for maximum framework-dealumination in accordance with electron-microprobe analyses is $Na_{0.27}K_{0.02}Ca_{0.02}Al_{2.27}[Al_{7.13}Si_{28.87}O_{72}]\cdot nH_2O$.

Extraframework Al

In contrast to previous studies (e.g., Yamamoto et al. 1996; Misaelides et al. 1996; Tsitsishivili 1978), our experiment suggests that the dissolved Al^{3+} from the framework surface is re-incorporated into the channels. The Al atoms in the channel bond to framework O atoms and channel H_2O oxygen atoms in distances close to the expected value of $Al^{[6]}$-O = 1.94 Å. The O-Al-O angles for Al1 and Al2 indicate a typical octahedral topology: 90° and 180° whereas the coordination of Al3 is only poorly defined. The Al sites in the channels are only very low-populated. The Al3 position reveals a decreasing population with dehydration, most probably related to decreasing bonding facilities with surrounding H_2O. Thus, the channel Al3 diffuses most probably to different positions which are not detectable due to high disorder and low populations. The channel Al of sample REE293 sums to 1.32 Al^{3+} pfu whereas DEHY378 reveals a total Al concentration of about 0.84 pfu. The population of individual channel Al sites in the investigated heulandite is in the range of ca. 10% or below. These Al sites are well defined and exhibit significantly lower B_{eq} values than H_2O or H_3O^+ molecules. However, the H_2O molecules completing the Al coordination are strongly disordered. Thus, Al-O(H_2O) distances and O-Al-O angles are associated with high uncertainty.

Nightingale (1959) reports a hydrated ionic radius for Al^{3+} of 4.75 Å whereas the corresponding radius for hydrated La^{3+} was given as 4.52 Å. Thus, on the first glance it seems surprising that Al was found as a significant extraframework component whereas REE were only analyzed in trace concentrations. However, one may argue that Al^{3+} never had to invade the heulandite channels from solution because Al^{3+} ions were dissolved by H_3O^+ already in the channels of heulandite and therefore inter-channel diffusion was very limited. Probably, the framework detached Al^{3+} ions immediately rearrange to more stable $[Al(H_2O)_6]^{3+}$ complexes and migrate to energetically favored channel sites.

On the other hand the hydrated radius of Mg^{2+} was reported to be 4.28 Å (Nightingale 1959) but Mg^{2+} can be incorporated into heulandite by corresponding exchange experiments (Stolz and Armbruster 1997). Thus the small ions (Mg^{2+} and Al^{3+}) may strip off part of their outer hydration sphere and may invade even narrow passages.

Of particular interest is the position of Al1 because it leads to edge-sharing between a framework tetrahedron (T5) and a partially occupied channel octahedron which appears highly unusual. If the framework tetrahedron (T5) was occupied by only Si, the repulsion between tetrahedral Si and edge-sharing octahedral Al would be probably too strong to allow such an arrangement. Because the population of Al1 is only ca. 10%

we suggest that this edge-sharing only occurs if T5 is locally occupied by Al. A rough estimate based on average T5-O distances (Table 4) suggests that T5 is occupied by more than 10% Al which agrees with the above hypothesis. However, there also must be sterical reasons governing the distribution of Al sites within the channels, since most of the octahedrally coordinated channel Al (Al1 and Al2) was closest to the relatively Si-rich tetrahedra T5, whereas no Al is close to the somewhat Al-richer tetrahedra T3 and only the low-populated Al3 site was close to the Al-rich tetrahedra T2. Another question of interest is whether $Al1O_6$ octahedra form edge-sharing strings parallel to b (Figs. 1 and 2), stabilizing the porous structure, or whether disordered single octahedra exist in the channels. The answers to these questions remain unclear because the population of the H_2O molecule WA6 (forming the common octahedral edge) strongly decreases with dehydration, and even in the most dehydrated sample (DEHY378) the population of WA6 (18%) is higher than that of Al1 (10%). These populations indicate that the WA6 site not only coordinates Al1 but may also be a favored position for hydrogen-bonded H_2O or H_3O^+ molecules. Similar arguments hold for WA9 forming the isolated apices of the Al1 octahedron. Single $Al1O_6$ octahedral units are also supported by bond-strength arguments. Double units would lead to a bond-strength sum of 1.0 valence units (v.u.) at the linking oxygen of WA6, which is too high for H_2O and for which Brown (1981) gives a base strength of 0.4 v.u. The presence of OH^- can be excluded under such acidic conditions. The Al2 site forms a $Al(H_2O)_6^{3+}$ complex in the center of the A channel. Similar H_2O complexes in heulandite have been resolved for Mg and Mn (Stolz and Armbruster 1997).

Under acidic pH conditions in siliceous tuffs, clay minerals form instead of zeolites. The latter are only known to form under alkaline pH conditions. In addition to the chemical differences between these two mineral groups, clays are characterized by mainly octahedral Al whereas zeolites have tetrahedral Al. Thus, one may speculate that acid-treated zeolites (heulandites) with beginning dealumination and re-incorporation of octahedral Al into the structural channels represent a metastable product toward clay formation. Solutions of very low pH are typical for mine-drainage waters (e.g., Zamzow and Schultze 1995). If heulandite-group zeolites are used for the purification of waste waters with low pH, dealumination and H^+ or H_3O^+ incorporation should be considered because it lowers the total effective ion-exchange capacity for the removal of metals in these contaminated waste waters.

REE uptake in heulandite

The very low La and Er uptake is probably related to the narrow free diameter of the channels. Heulandite has a free diameter of 2.4–6.1 (eight-membered ring C channel), 3.8–4.5 (eight-membered ring B channel), and 4.1–6.2 Å (ten-membered ring A channel) (Sherry 1969). Experiments on zeolites with larger channel diameters and different channel structures, e.g., faujasite or Linde Y (7.4 Å free channel diameter) yielded almost fully REE-exchanged products under similar conditions (Sherry 1969; Olson et al. 1968; Scherzer et al. 1975). Er^{3+} and La^{3+} in solution are apparently highly hydrated and the corresponding H_2O complexes are therefore too large for a high

mobility through the heulandite channels. Nightingale (1959) suggests a hydrated radius for La^{3+} of 4.5 Å in contrast to only 3.8 Å for Na^+, and 3.2 Å for Cs^+.

The REE La (195 ppm) and Er (656 ppm) in the exchange product are either incorporated in the structure or precipitated as finely crystalline $REECl_3$ salts and intermingled with heulandite. An average dimension for heulandite crystals of ca. 100 μm × 20 μm × 5 μm, and 656 ppm Er and 195 ppm La indicates 1.5 REE ions per $Å^2$ on the crystal surface. This value is unreasonable for single-layer surface adsorption due to the large REE ionic radii. If La and Er are precipitated as additional phases their different concentration may be interpreted by different solubility products of various hydrated $REECl_3$ salts. Because the pH increased during the exchange reaction, the latter interpretation cannot be excluded.

Furthermore, it is not yet understood why the Er content in the heulandite was three times higher than the La content. In previous studies on REE abundance in natural heulandite (e.g., Terakado and Nakajima 1995; Armbruster et al. 1996), the larger La ion showed a higher affinity to heulandite than the smaller Er ion. The difference between REE concentrations found in natural zeolites and REE incorporation in the laboratory is that in nature REE may be trapped during crystal growth, yielding no selectivity due to a sieving effect (channel opening).

REFERENCES CITED

Alberti, A. (1972) On the crystal structure of the zeolite heulandite. Tschermaks Mineralogische und Petrographische Mitteilungen, 18, 129–146.

Alberti, A. and Vezzalini, G. (1983) The thermal behaviour of heulandites: a structural study of the dehydration of the Nadap heulandite. Tschermaks Mineralogische und Petrographische Mitteilungen, 31, 259–270.

Alberti, A., Gottardi, G., and Lai, T. (1990) The determination of (Si,Al) distribution in zeolites. In D. Barthomeuf, Ed., Guidelines for Mastering the Properties of Molecular Sieves, p. 145–155. Plenum Press, New York.

Armbruster, T. and Gunter, M.E. (1991) Stepwise dehydration of heulandite-clinoptilolite from Succor Creek, Oregon, U.S.A.: a single-crystal X-ray study at 100 K. American Mineralogist, 76, 1872–1883.

Armbruster, T., Kohler, T., Meisel, T., Nägler, T.F., Götzinger, M.A., and Stalder, H.A. (1996) The zeolite, fluorite, quartz assemblage of the fissures at Gibelsbach, Fiesch (Valais, Switzerland): crystal chemistry, REE patterns, and genetic speculations. Schweizerische Mineralogische und Petrographische Mitteilungen, 76, 131–146.

Bresciani-Pahor, N., Calligaris, M., Nardin, G., Randaccio, L., Russo, E., and Comin-Chiaromonti, P. (1980) Crystal structures of a natural and partly Ag-exchanged heulandite. Journal of the Chemical Society. Dalton Transactions, Inorganic Chemistry, 1980, 1511–1514.

Bresciani-Pahor, N., Calligaris, M., Nardin, G., and Randaccio, L. (1981) Location of cations in metal ion-exchanged zeolites. Part 2. Crystal structures of a fully silver-exchanged heulandite. Journal of the Chemical Society. Dalton Transactions, Inorganic Chemistry, 1981, 2288–2291.

Brown, I.D. (1981) The bond-valence method: an empirical approach to chemical structure and bonding. In M. O'Keeffe and A. Navrotsky, Eds., Structure and Bonding in Crystals, vol. II, p. 1–30. Academic Press, New York.

Enraf-Nonius (1983) Structure determination package (SDP). Enraf-Nonius, Delft, The Netherlands.

Filippidis, A., Godelitsas, A., Charistos, D., Misaelides, P., and Kassoli-Fournaraki, A. (1996) The chemical behaviour of natural zeolites in aqueous environments: Interactions between low-silica zeolites and 1 M NaCl solutions of different initial pH-values. Applied Clay Science, 11, 199–209.

Godelitsas, A., Misaelides, P., Charistos, D., Filippidis, A, and Anousis, I. (1996a) Interaction of HEU-type zeolitic crystals with thorium aqueous solutions. Chemie der Erde, 56, 143–156.

Godelitsas, A., Misaelides, P., Filippidis, A., Charistos, D., and Anousis, I. (1996b) Uranium sorption from aqueous solutions on sodium-form of HEU-type zeolite crystals. Journal of Radioanalytical and Nuclear Chemistry, 208, 393–402.

Gottardi, G. and Galli, D. (1985) Natural Zeolites, 409 p., Springer Verlag, Berlin.

Gunter, M.A., Armbruster, T., Kohler, T., and Knowles, C.R. (1994) Crystal structure and optical properties of Na- and Pb-exchanged heulandite-group zeolites. American Mineralogist, 79, 675–682.

Hambley, T.W. and Taylor, J.C. (1984) Neutron diffraction studies on natural heulandite and partially dehydrated heulandite. Journal of Solid State Chemistry, 54, 1–9.

Johnson, C.K. (1970) The effect of thermal motion on interatomic distances and angles. In F.R. Ahmed, Ed., Crystallographic Computing, p. 220–226. Munksgaard, Copenhagen.

Kerr, G.T. (1969) Chemistry of crystalline aluminosilicates. VII. Thermal decomposition products of ammonium zeolite Y. Journal of Catalysis, 15, 200–204.

Kolodziejski, W., Delaude, L., Laszlo, P., Montaufier, M.-T., and Klinowski, J. (1993) Solid-state nuclear magnetic resonance studies of the transformation of the zeolite Y catalyst in the course of hydrochlorination of 1-methylcyclohexene by thionyl chloride. Applied Catalysis, 98, 71–79.

Koyama, K. and Takéuchi, Y. (1977) Clinoptilolite: the distribution of potassium atoms and its role in the thermal stability. Zeitschrift für Kristallographie, 145, 216–239.

Lundgren, J.-O. and Taesler, I. (1979) Orthorhombic oxonium hydrogenselenate. Acta Crystallographica, B35, 2384–2386.

Merkle, A.B. and Slaughter, M. (1968) Determination and refinement of the structure of heulandite. American Mineralogist, 53, 1120–1138.

Misaelides, P. and Godelitsas, A. (1995) Removal of heavy metals from aqueous solutions using pretreated natural zeolitic materials: the case of mercury (II). Toxicological and Environmental Chemistry, 51, 21–29.

Misaelides, P., Godelitsas, A., Link, F., and Baumann, H. (1996) Application of the $^{27}Al(p,\gamma)$ ^{28}Si nuclear reaction to the characterization of the near-surface layers of acid-treated HEU-type zeolite crystals. Microporous Materials, 6, 37–42.

Mumpton, F.A. (1988) Development of uses for natural zeolites: a critical commentary. In D. Kallo and H.S. Sherry, Eds., Occurrence, Properties, and Utilization of Natural Zeolites, p. 333–365. Akademiai Kiado, Budapest.

Nightingale, E.R. (1959) Phenomenological theory of ion solution. Effective radii of hydrated ions. Journal of Physical Chemistry, 63, 1381–1387.

Olson, D.H., Kokotailo, G.T., and Charnell, J.F. (1968) The crystal chemistry of rare earth faujasite-type zeolites. Journal of Colloid and Interface Science, 28, 305–314.

Scherzer, J., Bass, J.L., and Hunter, F.D. (1975) Structural characterization of hydrothermally treated lanthanum Y zeolites. I. Framework vibrational spectra and crystal structure. II. Infrared spectra in the hydroxyl stretching region and acid sites. Journal of Physical Chemistry, 79, 1194–1205.

Shannon, R.D. (1976) Revised effective ionic radii and systematic studies of interatomic distances in halides and chalcogenides. Acta Crystallographica, A32, 751–767.

Sherry, H.S. (1969) The ion-exchange properties of zeolites. In J.A. Marinsky, Ed., Ion Exchange: A series of advances, 2, p. 89–133. Marcel Dekker, New York.

Siemens (1994): SHELXTL Version 5.03, Siemens Analytical X-ray Instruments.

Stolz, J. and Armbruster, T. (1997) Mg^{2+}-, Mn^{2+}-, Cd^{2+}-, and Sr^{2+}-exchange in heulandite single-crystals: X-ray structure refinements. In Natural Zeolites '97, Program and Abstracts, p. 273–274. Ischia, Italy.

Sukheswala, R.N., Avasia, R.K., and Gangopadhay, M. (1974) Zeolites and associated secondary minerals in the Deccan Traps of Western India. Mineralogical Magazine, 39, 658–671.

Terakado, Y. and Nakajima, W. (1995) Characteristics of rare-earth elements, Ba, Sr, and Rb abundances in natural zeolites. Geochemical Journal, 29, 337–345.

Tsitsishivili, G.V. (1978) Adsorption and catalytic properties of some soviet natural zeolites. In L.B. Sand and F.A. Mumpton, Eds., Natural Zeolites: Occurrence, Properties, Use, p. 397–401. Pergamon Press, Oxford.

Yamamoto, S., Sugiyama, S., Matsuoka, O., Kohmura, K., Honda, T., Banno, Y., and Nozoye, H. (1996) Dissolution of zeolite in acidic and alkaline aqueous solutions as revealed by AFM imaging. Journal of Physical Chemistry, 100, 18474–18482.

Yang, P. and Armbruster, T. (1996) Na, K, Rb, and Cs exchange in heulandite single-crystals: X-ray structure refinements at 100 K. Journal of Solid State Chemistry, 123, 140–149.

——— (1998) X-ray single-crystal structure refinement of NH_4-exchanged heulandite at 100 K. European Journal of Mineralogy, 10, 461–471.

Zamzow, M.J. and Schultze, L.E. (1995) Treatment of acid mine drainage using natural zeolites. In D.W. Ming and F.A. Mumpton, Eds., Natural Zeolites '93: Occurrence, Properties, Use, p. 405–413. International Committee on Natural Zeolites, Brockport, New York.